Effect of strong acids on red mud structural and adsorption properties

Wentao Liang, Sara J. Couperthwaite*, Gurkiran Kaur, Cheng Yan, Dean W. Johnstone and Graeme J. Millar

[1)] Chemistry, Physics, Mechanical Engineering, Science and Engineering Faculty, Queensland University of Technology, GPO Box 2434, Brisbane Queensland 4001, Australia.

Fax: +61 7 3138 1804; Tel +61 7 3138 4766; E-mail: sara.couperthwaite@qut.edu.au

ABSTRACT

The removal of fluoride using red mud has been improved by acidifying red mud with hydrochloric, nitric and sulphuric acid. This investigation shows that the removal of fluoride using red mud is significantly improved if red mud is initially acidified. The acidification of red mud causes sodalite and cancrinite phases to dissociate, confirmed by the release of sodium and aluminium into solution as well as the disappearance of sodalite bands and peaks in infrared and X-ray diffraction data. The dissolution of these mineral phases increases the amount of available iron and aluminium oxide/hydroxide sites that are accessible for the adsorption of fluoride. The removal of fluoride is dependent on the charge of iron and aluminium oxide/hydroxides on the surface of red mud. Acidifying red mud with hydrochloric, nitric and sulphuric acid resulted in surface sites of the form $\equiv SOH_2^+$ and $\equiv SOH$. Optimum removal is obtained when the majority of surface sites are in the form $\equiv SOH_2^+$ as the substitution of a fluoride ion doesn't cause a significant increase in pH. This investigation shows the importance of having a low and consistent pH for the removal of fluoride from aqueous solutions using red mud.

KEYWORDS: acid stability, adsorption, bauxite residue, fluoride, red mud

INTRODUCTION

At the end of 2010, around 3 billion tonnes of bauxite refinery residue (red mud) had been produced globally using the Bayer process to convert aluminium oxides in bauxite ore to alumina.[1, 2] It is estimated that an additional 120 million tonnes is produced each year.[1, 2] The magnitude of waste generated by this industry clearly demonstrates the need for future developments that find a beneficial use for this material. Due to the complexity and classification (hazardous material under the Basel Convention)[3] of bauxite residue, numerous researchers are trying to utilise the waste residue in water purification applications.

Red mud (generally a slurry) is comprised of iron oxides, titanium oxides, silicon oxides and undissolved alumina, along with a wide range of other oxides depending on the country of origin.[4-6] Trace levels of metal oxides, such as arsenic, cadmium, chromium, copper, gallium, lead, mercury, nickel and in some cases thorium and uranium, are of particular concern.[7] Apart from heavy metal contamination, the alkalinity of red mud also constrains viable applications due to the cost of neutralisation. Alkalinity in the residue exists in both solid and solution as: 1) entrained liquor (sodium hydroxide, sodium aluminate and sodium carbonate), 2) calcium compounds, such as hydrocalumite, tri-calcium aluminate and lime, and 3) sodalite ($(NaAlSiO_4)_6(Na_2X)$), where X can be SO_4^{2-}, CO_3^{2-}, $Al(OH)_4^-$ or Cl^-).[8]

The potential environmental implications of seepage, dam failures and flooding can have a large negative impact on the surrounding water bodies, including groundwater, lakes and rivers, when soluble caustic chemicals are released. Mining industries employ precautionary measures to minimise environmental risks such as lining dams, however during natural disasters such as flooding there are no measures that can be taken to prevent spillage. Apart from the potential risks of tailing dams, there also exists the problem that large areas of land are being transformed into landfill to contain red mud residue. The discovery of a viable application (in-expensive and uses large quantities) for the reuse of red mud will significantly minimise environmental impacts caused by tailings dams and the associated costs of storage facilities (more than $80 million a year).[9]

In recent years, many researchers have focused on utilising red mud as an adsorbent material, and have had success in the adsorption of heavy metals,[10, 11] arsenate[12-17], phosphates[18-20] and to a lesser extent fluoride.[21-23] Fluoride is naturally found in

groundwater due to the dissolution of fluoride bearing minerals over long periods of time.[24] However, elevated levels of fluoride in groundwater can generally be traced back to a number of industries, including but not limited to, glass and ceramic production, electroplating, coal fired power stations, brick and iron works, and aluminium smelters.[21, 25] It is estimated that more than 200 million people rely on contaminated drinking water containing more than 1.5mg/L of fluoride (World Health Organisation safe level).[26] Continual and excess exposure to fluoride results in diseases such as osteoporosis, arthritis, brittle bones, cancer, infertility, brain damage, Alzheimer and thyroid disorders in humans.[21]

Traditionally, contaminated fluoride drinking waters have been treated using lime, which results in the precipitation of fluorite. However, due to the slight solubility of CaF_2, it is difficult to treat F^- levels below 20mg/L.[27] Other precipitating and coagulating reagents have been used and include iron (III), alum, calcium and activated alumina.[21] More involved processes, such as ion exchange, reverse osmosis and electrodialysis, have also been explored, but have subsequent waste disposal issues and high operating and maintenance costs.[21, 28]

Of particular interest, is the removal of fluoride using activated alumina and iron-based materials, schwertmannite ($Fe_8O_8(OH)_6(SO_4)\cdot nH_2O$), granular ferric hydroxide ($Fe(OH)_3$), and goethite(α-FeOOH),[21, 28] as they are found in red mud and thus suggest red mud can potentially be an adsorbent. Fluoride sorption using iron-based sorbents is facilitated by exchange reactions involving F^- and OH^- with FeOH surface groups. A maximum Langmuir adsorption capacity of 0.368 mmol/g of fluoride on granular ferric hydroxide has been reported by Kumar et al.,[29] in the pH range 6.0 to 7.0. Phosphate and sulphate (inner-sphere forming species) have been shown to have negative effects on the loading capacity of fluoride, while outer-sphere forming species (chloride and nitrate) improved fluoride removal slightly.[21] At pH values less than 3.7, fluoride removal generally decreases due to the formation of AlF_x soluble species, while in alkaline solutions OH^- displaced F^-.[30] A study by Cengeloglu et al.[23] investigated the adsorption capacity of untreated and hydrochloric treated red mud. The maximum removal capacity was obtained using the acid treated red mud and observed a Langmuir loading capacity of 0.331 mmol/g at pH 5.5 after 2 hour equilibration. Granular red mud prepared by Tor et al.,[31] exhibited a Langmuir loading capacity of 0.339 mmol/g at pH 4.7 after 6 hours equilibration during a batch trial. Previous

studies have also shown that the spent red mud satisfies the toxicity characteristic leaching procedure (TCLP) used to classify inert wastes.[31]

The majority of papers in this field of research focus on the use of hydrochloric acid to activate red mud, however this can reduce the iron content available for subsequent adsorption applications. Consequently, this investigation will assess the structural changes and resulting adsorption capacities of Australian red mud untreated and treated with hydrochloric, nitric and sulphuric acid. Particular emphasis will be placed upon determining the reactions involved during acid activation and how the remaining mineralogical composition correlates with fluoride removal efficiencies.

MATERIALS AND METHODS

Acid activated red mud

Red mud from an Australian alumina refinery was dried over a period of 2 days at 105°C before being crushed to a fine powder using an agate ball mill. Using a Retsch AS200 sieving stack consisting of 10 sieves, ranging from 4mm to 64µm, red mud was processed to give a size fraction < 250µm. Known concentrations of hydrochloric (HCl), nitric (HNO_3) and sulphuric (H_2SO_4) acid were prepared from concentrated AR reagents (Rowe Scientific). Red mud (12.5g) was measured into 250mL Nalgene bottles and then reacted with 200mL of DI water and each acid. Each bottle was placed on a Ratek rotary stirrer for 1 hour at 200rpm. These samples were subsequently centrifuged at 400rpm for 10 min using a C2041 Centurion centrifuge. The red mud was placed in the oven to dry (90°C), while the solution was stored for analysis.

Fluoride adsorption

The 100ppm fluoride solutions were prepared using AR grade sodium fluoride purchased from Sigma-Aldrich. Adjustment of the pH was achieved using a transfer pipette to add 1M nitric acid dropwise while the pH was monitored with a TPS WP40 pH meter and Sentek laboratory probe. To 12, 50mL centrifuge tubes, a known amount of acid activated red mud (ranging from 0.025 to 2.000g) was added followed by the addition of 40mL of the 100mg/L fluoride solution. The centrifuge tubes were then placed on a rotary stirrer at 200rpm for 2 hours. After equilibrium was reached, the tubes were removed from the rotary stirrer and subsequently centrifuged at 400rpm for 10 min using a C2041 Centurion centrifuge. The red

mud was placed in the oven to dry (90°C), while the solution was stored for analysis. The supernatant was kept for fluoride analysis using a fluoride ion selective electrode (ISE).

Characterisation techniques

Fluoride analysis was obtained using a TPS uniPROBE Fluoride (F-) ISE. A fluoride ISE buffer was prepared using 1 M of sodium chloride (NaCl) and 1 M sodium citrate dehydrate ($Na_3C_6H_5O_7 \cdot 2H_2O$) dissolved in approximately 1.5 L deionised water. Sodium hydroxide (NaOH) was use to adjust the solution pH to 5.5 before making the solution up to 2 L. Calibration standards of 1, 10, 100, 1000 mg / L fluoride stock solutions were prepared from AR grade sodium fluoride (NaF). The electrode was calibrated with standards in the range of the sample. Standards and samples were analysed by combining 10 mL of the calibration standard solution (or sample) and 10 mL of the buffer solution whilst being stirred. The concentration of fluoride was then measured using the fluoride ISE.

X-Ray diffraction patterns were collected using a Philips X'pert wide angle X-Ray diffractometer, operating in step scan mode, with Co Kα radiation (1.7903 Å). Patterns were collected in the range 5 to 90° 2θ with a step size of 0.02° and a rate of 30s per step. Samples were prepared as Vaseline thin films on silica wafers, which were then placed onto aluminium sample holders. The XRD patterns were matched with ICSD reference patterns using the software package HighScore Plus. The profile fitting option of the software uses a model that employs twelve intrinsic parameters to describe the profile, the instrumental aberration and wavelength dependent contributions to the profile.

Samples of the residual acid solutions, after centrifugation, were analysed using an Agilent ICP-MS 7500CE instrument. The samples were diluted by a factor of 20 using a Hamilton dilutor with 10 and 1mL syringes. A certified standard from Australian Chemical Reagents (ARC) containing 1000ppm of aluminium, magnesium, calcium, iron and sodium were diluted to form a multi-level calibration curve and an external reference that was used to monitor instrument drift and accuracy of the results obtained. Results were obtained using an integration time of 0.15 seconds with 10 replications. Calibration curves had an r^2 value of 0.998 or higher.

Infrared spectra were obtained using a Nicolet Nexus 870 Fourier Transform infrared spectrometer (FTIR) with a smart endurance single bounce diamond ATR (attenuated total reflectance) cell. Spectra over the 4000-525 cm^{-1} range were obtained by the co-addition of 64 scans with a resolution of 4 cm^{-1} and a mirror velocity of 0.6329 m/s.

2.0 RESULTS AND DISCUSSION

2.1 Elemental and mineralogical composition

The elemental composition of this Australian red mud comprised of predominately iron (Fe_2O_3), titanium (TiO_2) and aluminium (Al_2O_3 and AlO(OH)) mineralogical compounds. Although the elemental analysis of red mud has been reported in numerous papers, the composition of each red mud sample differs, due to the original composition of the bauxite ore and the operating conditions used to extract alumina. The elemental abundance in bauxite residues generally follow Fe > Si ~ Ti > Al > Ca > Na.[32] The red mud used in this work has a particularly high content of aluminium, suggesting that the operating conditions were not optimised. The phase composition of untreated red mud (Figure 1) comprised of majorly hematite (Fe_2O_3), gibbsite ($Al(OH)_3$), boehmite (γ-AlO(OH)), sodalite ($Na_8(Al_6Si_6O_{24})Cl_2$ or $Na_8(Al_6Si_6O_{24})CO_3$), TiO_2 (anatase and rutile), quartz (SiO_2) and possibly cancrinite ($Na_6Ca_2Al_6Si_6O_{24}(CO_3)_2$). These mineralogical phases agree with the elemental analysis results (Table 1). The broadness of the peaks in the XRD pattern align with the following remarks from Grafe et al.,[32] that approximately 70% (by weight) of bauxite phases are crystalline, while the remaining 30% are amorphous materials.

A comparison of the washed and acid treated red mud XRD patterns (Figure 2) shows some phase intensity changes, and suggests that a portion of the mineralogical phases are unstable in acidic media. In particular, the sodalite peaks at around 16.2, 28.1 and 40.2 °2θ significantly decrease in intensity indicating the dissolution of this phase. Multiple decreases in intensities are observed between 30 and 35 °2θ, and are associated with quartz (HNO_3 and H_2SO_4 predominately) and cancrinite. It appears that 0.5M acid solutions have a limited effect on the overall mineralogical structure of iron and titanium oxide phases. This is ideal, as a high iron content in red mud has been found to be beneficial in the removal of fluoride.[23]

2.2 Leachants (ICP and reactions)

2.2.1 SEM-EDX

A comparison of the amount of Al, Na, Si and Ti to the amount of Fe in the washed and acid treated red muds is provided in Table 1. Interestingly, a higher concentration of acid doesn't necessarily mean that a greater amount of a particular element will be removed from the solid phase. In the case of HCl and H_2SO_4, the 0.5M acids had a greater effect on the dissolution of compounds containing aluminium, sodium and/or silica than their respective concentrated acid counterparts. This can be explained by the formation of additional phases between the dissolution species and excess Cl^- ions when using concentrated HCl, for example that forms NaCl. This is confirmed by XRD (Figure 2), which showed halite peaks (~ 36.9 °2θ). The SEM image of red mud reacted with concentrated HCl (Figure 3) also clearly shows the formation of an addition mineralogical phase, and based on the XRD pattern it can be assumed that halite (NaCl) has coated the exterior of the red mud particles. The formation of this phase is not expected to hinder the removal of fluoride as it is highly soluble, however due to its solubility it will increase the salinity of any treated solutions.

2.2.2 ICP-MS

After the treatment of red mud with each of the 1M acids, the filtrate was analysed using ICP-MS to determine the concentration of major ions being released into solution (Figure 4). It was found that sodium containing compounds are the most susceptible to acidic solutions. An increase in Na^+ is also observed for the washed red mud sample indicating that about a third of sodium released into solution is due to the dissolution of residual NaOH or NaOH trapped in sodalite aggregates. The general formula for sodalite is $Na_8(Al_6Si_6O_{24})CO_3$, which has a Na:Al mole ratio of 1.3. By subtracting the amounts of Na and Al ions released by the dissolution of NaOH (based on red mud washed values) from the concentrations of ions in the leachant solution of HCl, H_2SO_4 and HNO_3 gives the following Na:Al ratios: 1.52, 1.26 and 1.27, respectively. This indicates that the majority of sodium and aluminium ions released in solution are due to the dissolution of sodalite. A lower amount of sodium is released into solution for HCl treated red mud due to the formation of NaCl. The release of calcium is proposed to be due to Ca substituted sodalite and/or cancrinite ($Na_6Ca_2Al_6Si_6O_{24}(CO_3)_2$). The dissolution of sodalite is predicted to form the following products:[33]

Equation 1

$Na_8(Al_6Si_6O_{24})CO_3 + 13H_2SO_4 \rightarrow 4Na_2SO_4 + 3Al_2(SO_4)_3 + 6Si(OH)_4 + H_2O + CO_2\uparrow$

Equation 2

$Na_8(Al_6Si_6O_{24})CO_3 + 24HCl \rightarrow 8NaCl + 6AlCl_3 + 6Si(OH)_4 + H_2O + CO_2\uparrow$

Equation 3

$Na_8(Al_6Si_6O_{24})CO_3 + 24HNO_3 \rightarrow 8Na(NO_3) + 6Al(NO_3)_3 + 6Si(OH)_4 + H_2O + CO_2\uparrow$

2.3 Infrared Spectroscopy

2.3.1 Red mud

Infrared spectroscopy has been used to monitor changes in bonding environments of the numerous components of red mud with the addition of different acids. These changes include both shifts in band position (strength of bonds) and also decreases/increases in intensity due to the dissolution/formation of phases. Washed red mud (Figure 5) will be used as a baseline to any changes that have occurred with the addition of different strengths of acid. A broad band between 3650 and 3000 cm^{-1} is associated with multitude overlapping hydroxyl-stretching bands, in particular metal-OH groups and water. Based on the XRD pattern of red mud it is believed that the multiple of bands between 3650 and 3300 cm^{-1} are due to the ν(OH) stretching modes of gibbsite.[34-36] Boehmite peaks are observed at around 3235 and 3124 cm^{-1}.[34, 35] Bands associated with surface hydroxyl groups of hematite appear in the range 3700, 3635, 3490, 3435 and 3380cm^{-1}.[37] In many cases these bands are not observed because the surface hydroxyl groups are removed during the drying process. The overall broadness of the band is due to multiple water stretching modes. Corresponding water bending modes are observed as a low intensity broad peak centred at 1655 cm^{-1}.

In the lower wavenumber region, several bands are observed between 1550 and 1350 cm^{-1}, predominately due to carbonate ions in different bonding environments. The only carbonate containing minerals identified in the XRD patterns are sodalite and cancrinite, however some form of carbonate mineral may also be present in the amorphous content of red mud. The most intense peak in the infrared spectrum (987 cm^{-1}) is believed to be due to stretching vibrations of Si(Al)-O in sodalite and cancrinite.[38] The small band at 696 cm^{-1} is also thought to be associated with the Si-O-Al framework of sodalite.[39] It is also possible that nitrate is incorporated in these cage structures due to the presence of bands at around 1430 cm^{-1}.[40]

2.3.2 Acid treated red mud

The dissolution of sodalite (disappearance of the intense band at 987 cm^{-1} and the bands between 1400 and 1500 cm^{-1}) is clearly observed in Figure 6 with the addition of hydrochloric acid. These observations coincide with the interpretation of the elemental analysis and the proposed dissolution reactions. In the absence of sodalite, bands associated with Si-O vibrations (possibly quartz) are observed at 1036 cm^{-1}, which gradually decreases and is confirmed by XRD patterns. The band profile also indicates the formation of $SiO_2 \cdot xH_2O$ (formed from dissolved silica – $Si(OH)_4$), which has characteristic bands at 800 (w), 948 (w), 1090 (vs) 1190 (s,sh) and 3330 cm^{-1}(m).[41] This dissolution product appears to be relatively stable. Minimal changes in the higher wavenumber region indicates that the major iron and aluminium oxide/hydroxide components of red mud remain relatively unscathed until the concentration of acid reached 1M (significant decrease in intensity suggesting the initial stages of dissolution).

The infrared spectra of red mud treated with nitric acid (Figure 7) and sulphuric acid (Figure 8) show many similar bands as those described for hydrochloric acid treated red mud. Nitric acid treated red mud showed additional bands at 1406 and 1352cm^{-1} due to Al hydroxylated nitrate and ν_3 NO_3^- co-adsorbed with H_2O on the red mud particles, respectively.[40] Sulphuric acid treated red mud also showed an additional band (broad shoulder on the 1074 cm^{-1}) ascribed to sulphate vibrational modes found in the dissolution product thenardite (Na_2SO_4). The broadness of the higher wavenumber region is proposed to be water adsorbed to thenardite.

2.4 Removal of fluoride using acid treated red mud

The effect of acid activated red mud and pH on the removal of fluoride from aqueous solutions was investigated and found that red mud treated with sulphuric acid has the greatest efficiency in fluoride removal (approximately 70% removed from an initial concentration of 100ppm), independent of the initial solution pH (Figures 9 and 10). It is clear from the results that the best removal percentages are achieved at low pH < 4.5. The study by Cengeloglu et al.,[23] reported similar removal percentages using red mud, however maximum adsorption was reported to occur at a pH around 5.5. Deviations in results between the studies are believed to be due to the different activation processes used.

The removal mechanism of fluoride using red mud primarily involves neutral (≡SOH) and protonated ($\equiv SOH_2^+$) sites on the oxide/hydroxide components (such as hematite and gibbsite) when the pH is less than 7.[42] The increased removal efficiencies of acid treated red mud compared to washed red mud are consistent with the protonation of the surface hydroxyl groups (Equation 4). Increased removal efficiencies for sulphuric acid treated red mud are due to 2 protons being available to protonate the surface hydroxyl groups.

Equation 4

$\equiv SOH + H^+ \rightarrow \equiv SOH_2^+$

The benefit of the protonated sites in acid treated red mud is that the replacement of a proton (H^+) with fluoride (F^-) releases water (Equation 5), while the substitution of a proton with a neutral site (Equation 6) releases a hydroxyl unit and in turn causes the pH to rise. This is observed for the DI washed red mud sample (neutral pH and thus has ≡SOH sites) that showed promising removal efficiencies at low mass to volume ratios, however with the continued release of OH^- units, as F^- ions are adsorbed, the pH became alkaline and resulted in the deprotonation of the surface sites ($\equiv SO^-$), Equation 7. This can be further confirmed by comparing the removal efficiencies of washed red mud; whereby the fluoride solution with an initial pH of 4.75 showed reasonable fluoride adsorption (approximately 35%) followed by a sharp decrease as the pH rose above 6 (Figure 9), while a maximum of 10% fluoride removal is observed for the fluoride solution with an initial pH of 8 (Figure 10). Fluoride adsorption is hindered when the pH is greater than 6 because of the increasing repulsive forces between the negatively charged surface ($\equiv SO^-$) and fluoride ions.

Equation 5

$\equiv SOH_2^+ + F^- \rightarrow \equiv SF + H_2O$

Equation 6

$\equiv SOH + F^- \rightarrow \equiv SF + OH^-$

Equation 7

$\equiv SOH + OH^- \rightarrow \equiv SO^- + H_2O$

The efficiency of fluoride adsorption is highly dependent on the pH and any fluctuations in pH. This is clearly observed in Figure 10 for the adsorption of fluoride using sulphuric acidified red mud. This relationship shows that for consistent fluoride adsorption, a constant

pH needs to be maintained to avoid any sudden shocks to the surface adsorption sites. It is also highly possible that the formation of AlF_x complexes, in particular aluminium trifluoride (AlF_3), occurs when the pH of solution is less than 4. The formation of AlF_3 would account for some of fluctuations in fluoride removal percentages. The study by Cengeloglu et al.,[23] reported a decline in fluoride removal at pH below 4 and did not report the formation of any of these AlF_x phases. This could be accounted for the difference in the quantity of gibbsite of the different red mud sources used, whereby this study had a greater amount of Al_2O_3 (24.0%) than Cengeloglu (18.7%)[23]. The formation of this phase is a result of gibbsite in red mud reacting with HF that forms under these highly acidic conditions (Equation 9).

Equation 9

$$Al_2O_3 + 6HF \rightarrow 2AlF_3 + 3H_2O$$

CONCLUSIONS

Red mud is comprised of a number of mineralogical phases, however the most important phases in the removal process are hematite and gibbsite. The treatment of red mud with acid improved the adsorption properties of red mud in 2 ways: 1) transformed $\equiv SOH$ / $\equiv SO^-$ sites to $\equiv SOH_2^+$ and 2) increased the availability of metal oxide/hydroxide sites through the removal of sodalite and cancrinite phases. In order to achieve reasonable removal efficiencies for fluoride a pH < 4.5 needs to be maintained, with sulphuric acid producing the best removal efficiencies. Red mud treated with sulphuric acid gave the best removal efficiencies for fluoride due to 2 protons being available to protonate the surface hydroxyl groups. Sudden changes in pH have shown to have negative effects on the removal efficiencies and thus need to be controlled.

ACKNOWLEDGEMENTS

The financial and infra-structure support of the Energy and Process Engineering Discipline of the Science and Engineering Faculty and the Institute of Future Environments, Queensland University of Technology is gratefully acknowledged. The Australian Research Council (ARC) is thanked for funding some of the instrumentation used in this study (DE120101890). This study could also not have been completed without the support of the technical services team at QUT who ensured the analytical instrumentation was available to us.

REFERENCES

[1] A.R. Hind, S.K. Bhargava, S.C. Grocott, Colloids Surf., A 146 (1999) 359.
[2] N.C.R. Oeberg, E.H. Steinlechner, Light Met. (Warrendale, Pa.) (1996) 67.
[3] L. Fergusson, Light Met. (Warrendale, PA, U. S.) (2007) 105.
[4] K. Snars, R.J. Gilkes, Appl. Clay Sci. 46 (2009) 13.
[5] S. Baseden, D. Grey, Marine Pollution Bulletin 7 (1976) 4.
[6] K. Snars, R.J. Gilkes, Applied Clay Science 46 (2009) 13.
[7] R.S. Thakur, B.R. Sant, J. Sci. Ind. Res. 42 (1983) 87.
[8] R. Courtney, in: Residue Solutions Pty Ltd, 2007.
[9] P. Brecht, Nurs Stand 11 (1997) 20.
[10] R. Apak, E. Tütem, M. Hügül, J. Hizal, Water Research 32 (1998) 430.
[11] L. Santona, P. Castaldi, P. Melis, Journal of Hazardous Materials 136 (2006) 324.
[12] H. Genc, J.C. Tjell, J. Phys. IV 107 (2003) 537.
[13] H. Genc, J.C. Tjell, D. McConchie, O. Schuiling, J. Colloid Interface Sci. 264 (2003) 327.
[14] H. Genc-Fuhrman, Dan. Kemi 85 (2004) 42.
[15] H. Genc-Fuhrman, D. McConchie, O. Schuiling, in: 32nd International Geological Congress; A. A. Balkema, Florence, Italy, 2005, 223.
[16] H. Genc-Fuhrman, J.C. Tjell, D. McConchie, Environ. Sci. Technol. 38 (2004) 2428.
[17] H. Genc-Fuhrman, J.C. Tjell, D. McConchie, J. Colloid Interface Sci. 271 (2004) 313.
[18] B. Koumanova, M. Drame, M. Popangelova, Resources, Conservation and Recycling 19 (1997) 11.
[19] C.J. Liu, Y.Z. Li, Z.K. Luan, Z.Y. Chen, Z.G. Zhang, Z.P. Jia, J. Environ. Sci. (Beijing, China) 19 (2007) 1166.
[20] Y. Zhao, Q. Yue, Q. Li, X. Xu, Z. Yang, X. Wang, B. Gao, H. Yu, Chem. Eng. J. (Amsterdam, Neth.) 193-194 (2012) 161.
[21] A. Bhatnagar, E. Kumar, M. Sillanpaeae, Chem. Eng. J. (Amsterdam, Neth.) 171 (2011) 811.
[22] L. Stoica, C. Constantin, C. Calin, Sci. Bull. - Univ. Politeh. Bucharest, Ser. B 74 (2012) 87.
[23] Y. Cengeloglu, E. Kir, M. Ersoz, Sep. Purif. Technol. 28 (2002) 81.
[24] D. Banks, C. Reimann, O. Roeyset, H. Sharphagen, O.M. Saether, Appl. Geochem. 10 (1995) 1.
[25] F. Shen, X. Chen, P. Gao, G. Chen, Chem. Eng. Sci. 58 (2003) 987.
[26] W.H.O., Guidelines for drinking water quality. Geneva, 2004.
[27] C.L. Parker, C.C. Fong, Ind. Wastes (Chicago) 21 (1975) 23.
[28] S. Ayoob, A.K. Gupta, V.T. Bhat, Crit. Rev. Environ. Sci. Technol. 38 (2008) 401.
[29] E. Kumar, A. Bhatnagar, M. Ji, W. Jung, S.H. Lee, S.J. Kim, G. Lee, H. Song, J.Y. Choi, J.S. Yang, B.H. Jeon, Water Res. 43 (2009) 490.
[30] H. Farrah, J. Slavek, W.F. Pickering, Aust. J. Soil Res. 25 (1987) 55.
[31] A. Tor, N. Danaoglu, G. Arslan, Y. Cengeloglu, J. Hazard. Mater. 164 (2009) 271.
[32] M. Grafe, G. Power, C. Klauber, in: C. Minerals, Karawara, WA, Australia, 2009.
[33] S. Fortin, R. Breault, in: P. Watkinson, H. Mueller-Steinhagen, in: Engineering Conferences International, Sante Fe, New Mexico, 2003.
[34] V.C. Farmer, Editor, Mineralogical Society Monograph 4: The Infrared Spectra of Minerals. Mineral. Soc., 1974.
[35] S.J. Palmer, B.J. Reddy, R.L. Frost, Spectrochim. Acta, Part A 71A (2009) 1814.
[36] E. Balan, M. Blanchard, J.-F. Hochepied, M. Lazzeri, Phys. Chem. Miner. 35 (2008) 279.
[37] C.H. Rochester, S.A. Topham, J. Chem. Soc., Faraday Trans. 1 75 (1979) 1073.
[38] P. Castaldi, M. Silvetti, S. Enzo, P. Melis, Journal of Hazardous Materials 175 (2010) 172.
[39] P. Castaldi, M. Silvetti, L. Santona, S. Enzo, P. Melis, Clays Clay Miner. 56 (2008) 461.
[40] M.W. Ross, T.C. DeVore, in: (Ed.)^(Eds.); American Chemical Society, 2008, 6609.

[41] F.A. Miller, C.H. Wilkins, Anal. Chem. 24 (1952) 1253.
[42] P.K. Raul, R.R. Devi, I.M. Umlong, S. Banerjee, L. Singh, M. Purkait, J. Nanosci. Nanotechnol. 12 (2012) 3922.

LIST OF TABLES

LIST OF FIGURES

445 **Table 1**

Red mud treatment	Al:Fe	Na:Fe	Si:Fe	Ti:Fe
DI water	1.27	1.04	0.73	0.22
Conc. HCl	0.98	1.04	0.71	0.21
0.5M HCl	0.58	0.27	0.22	0.22
Conc. HNO_3	0.76	0.27	0.41	0.19
0.5M HNO_3	0.96	0.57	0.40	0.22
Conc. H_2SO_4	1.07	0.97	0.73	0.00
0.5M H_2SO_4	0.82	0.37	0.32	0.18

446

447

448 **Figure 1**

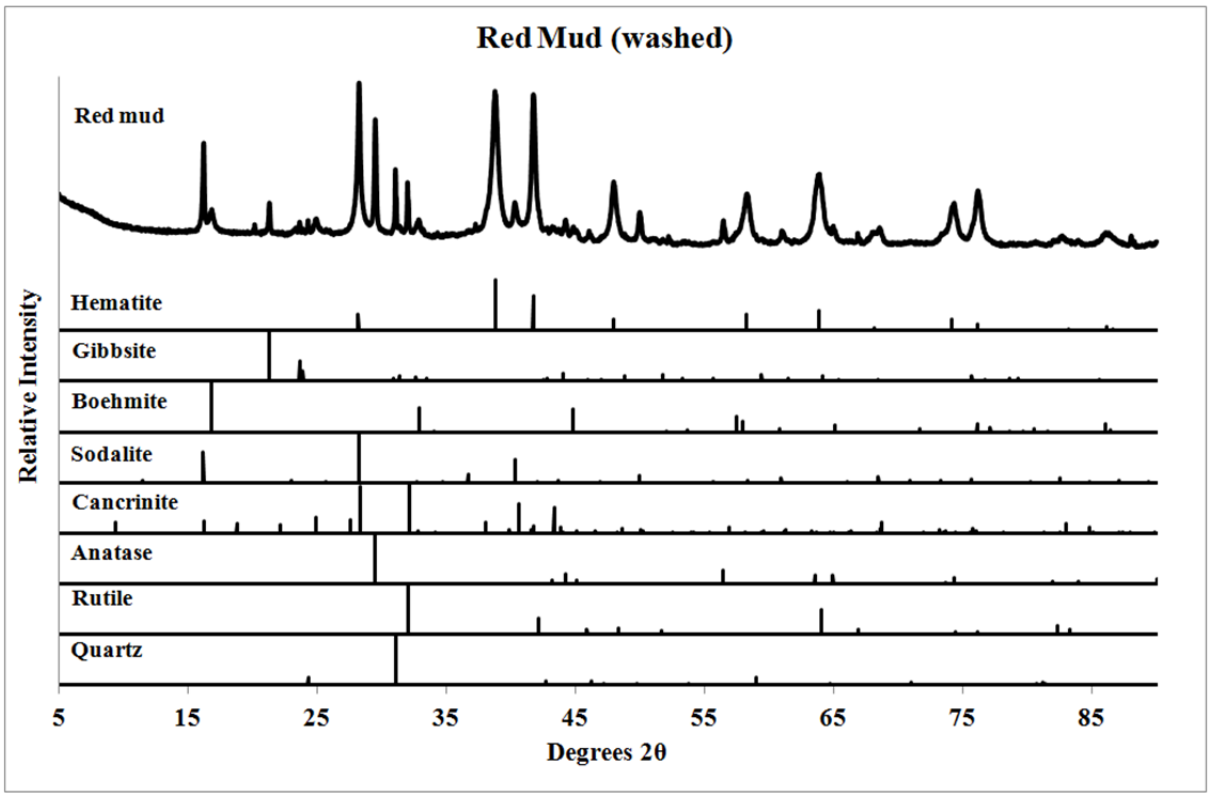

449

450

451 **Figure 2**

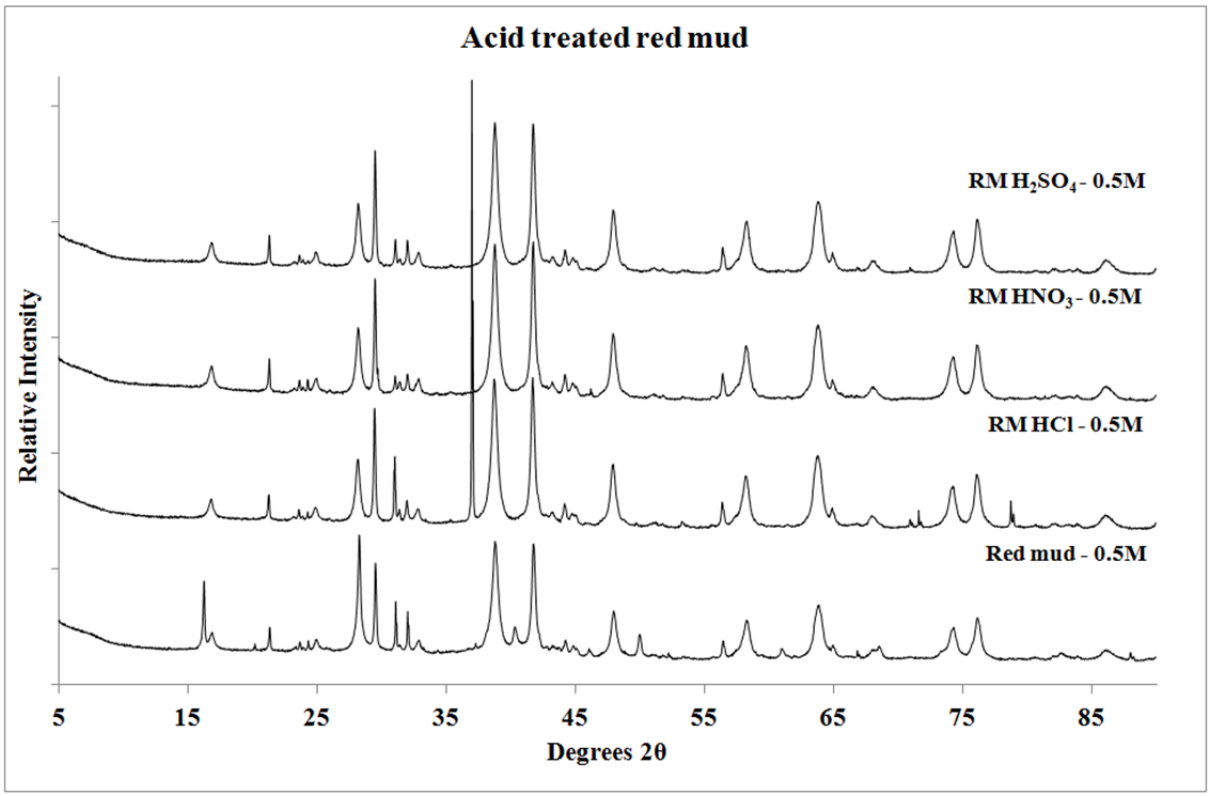

452

453

Figure 3

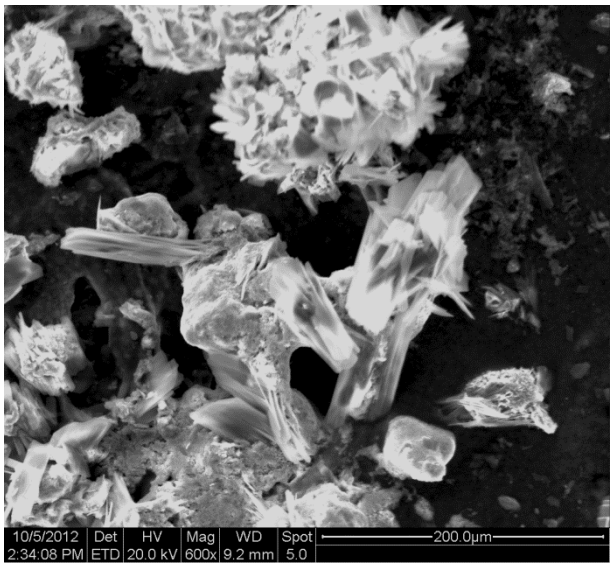

Figure 4

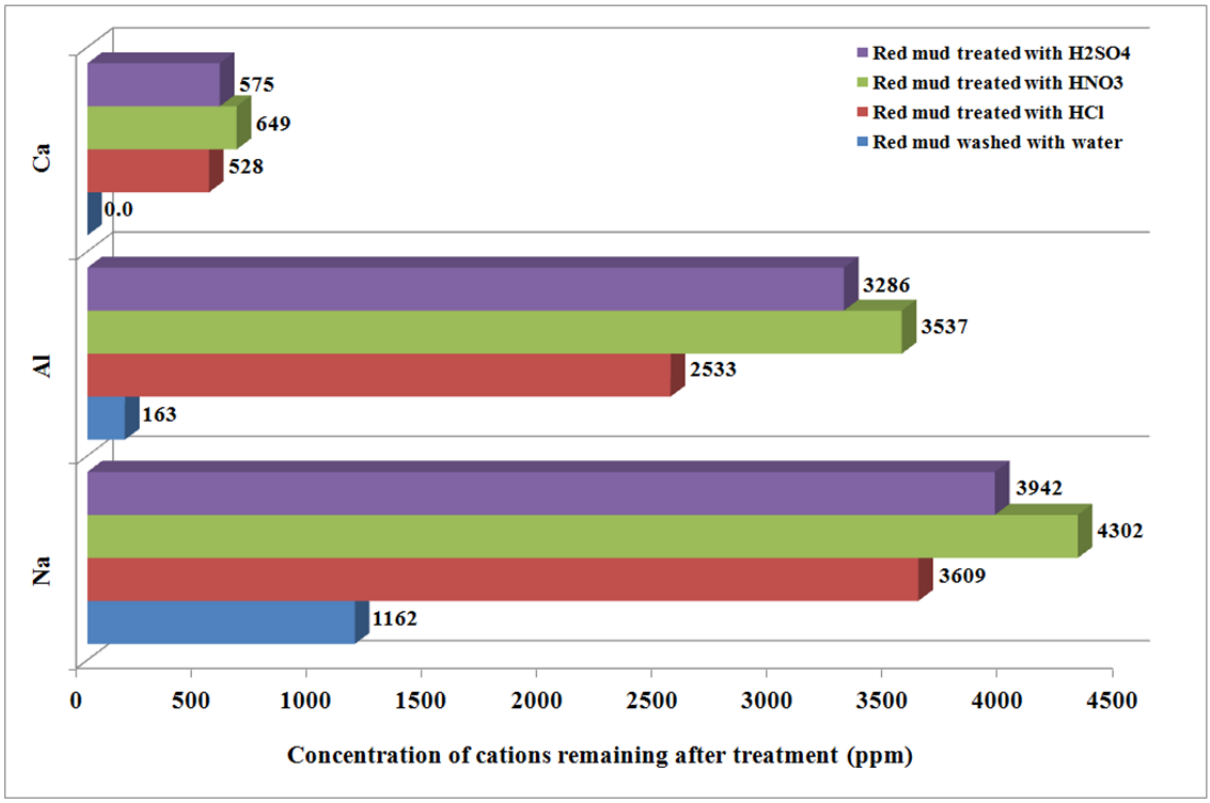

Figure 5

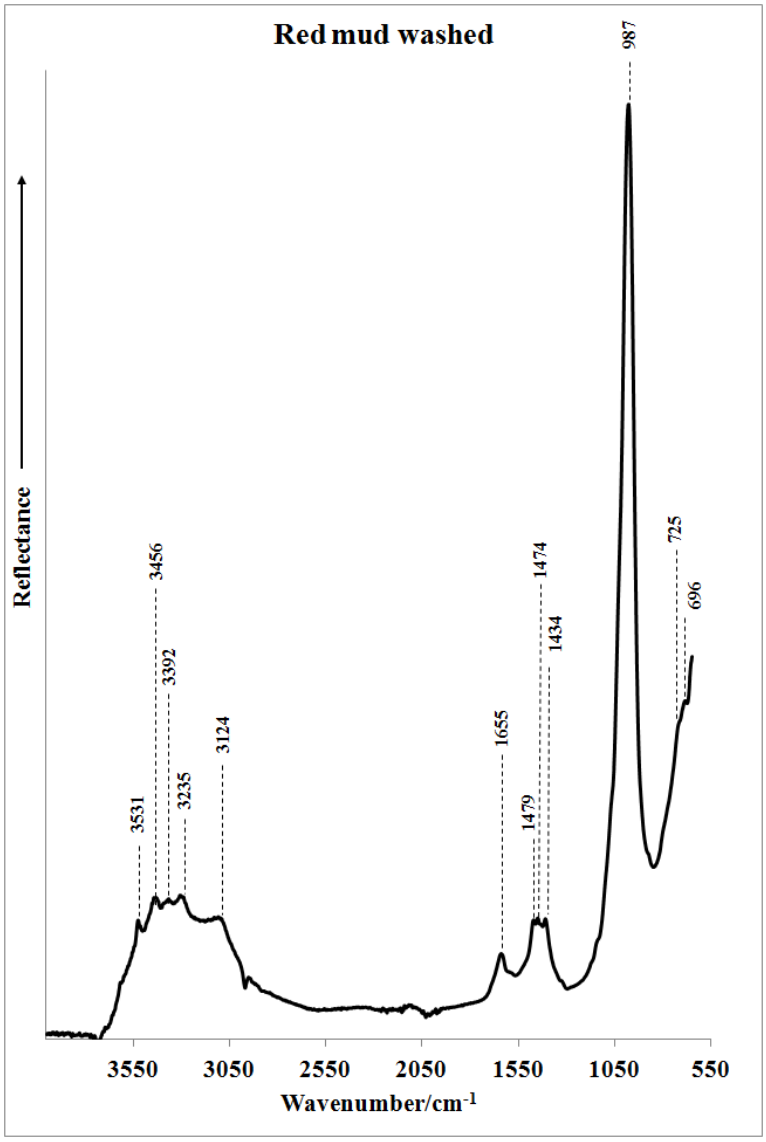
Red mud washed
Reflectance
3531
3456
3392
3235
3124
1655
1479
1474
1434
987
725
696
3550
3050
2550
2050
1550
1050
550
Wavenumber/cm-1

Figure 6

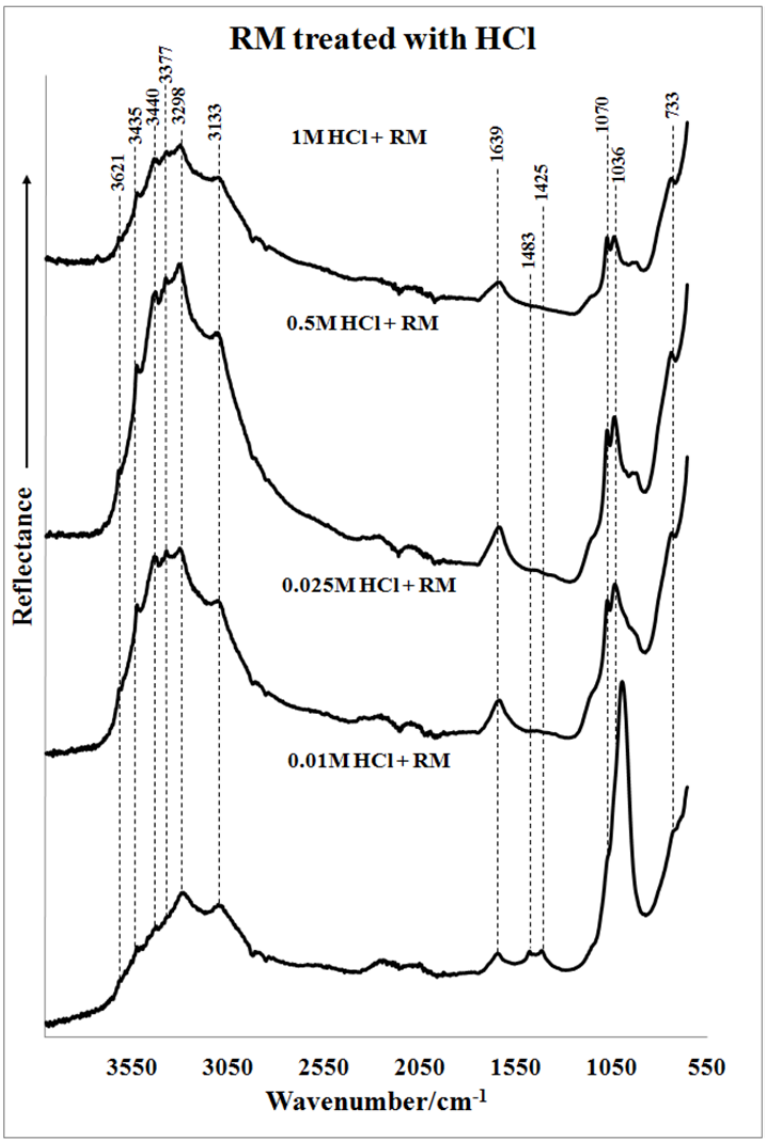
RM treated with HCl
3621
3435
3440
3377
3298
3133
1639
1483
1425
1070
1036
733
1M HCl + RM
0.5M HCl + RM
0.025M HCl + RM
0.01M HCl + RM
Reflectance
3550
3050
2550
2050
1550
1050
550
Wavenumber/cm-1

474 **Figure 7**

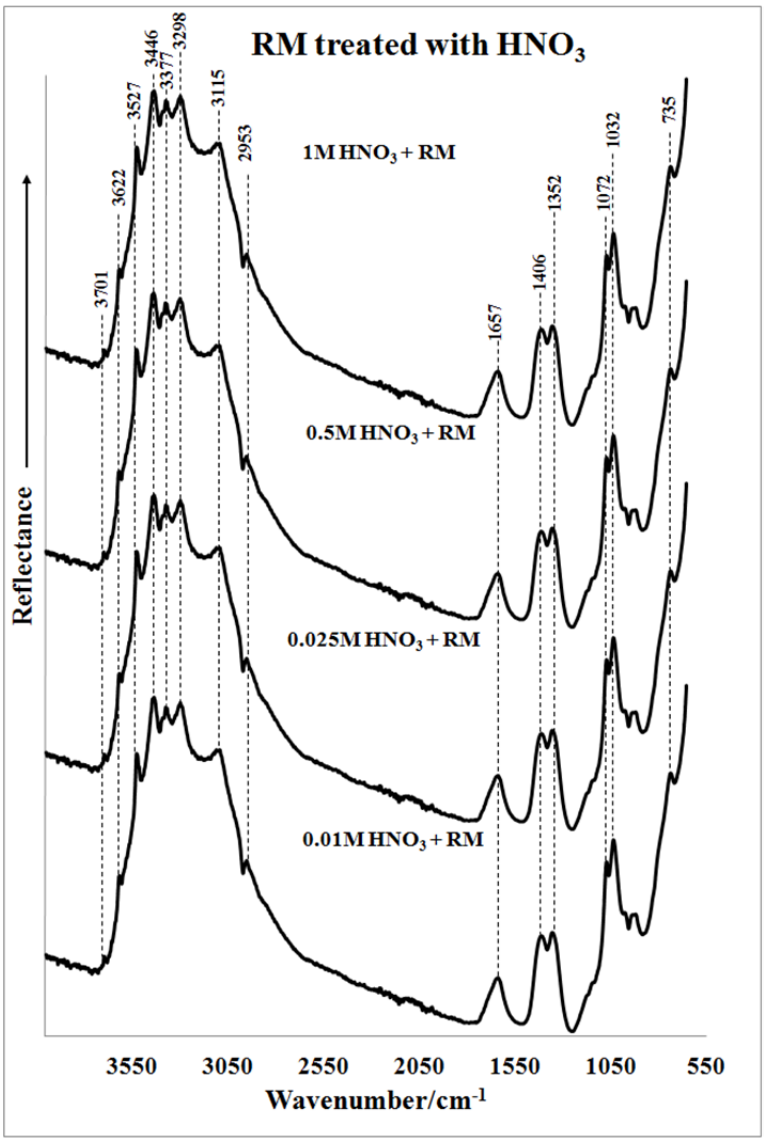

475

476

477

478 **Figure 8**

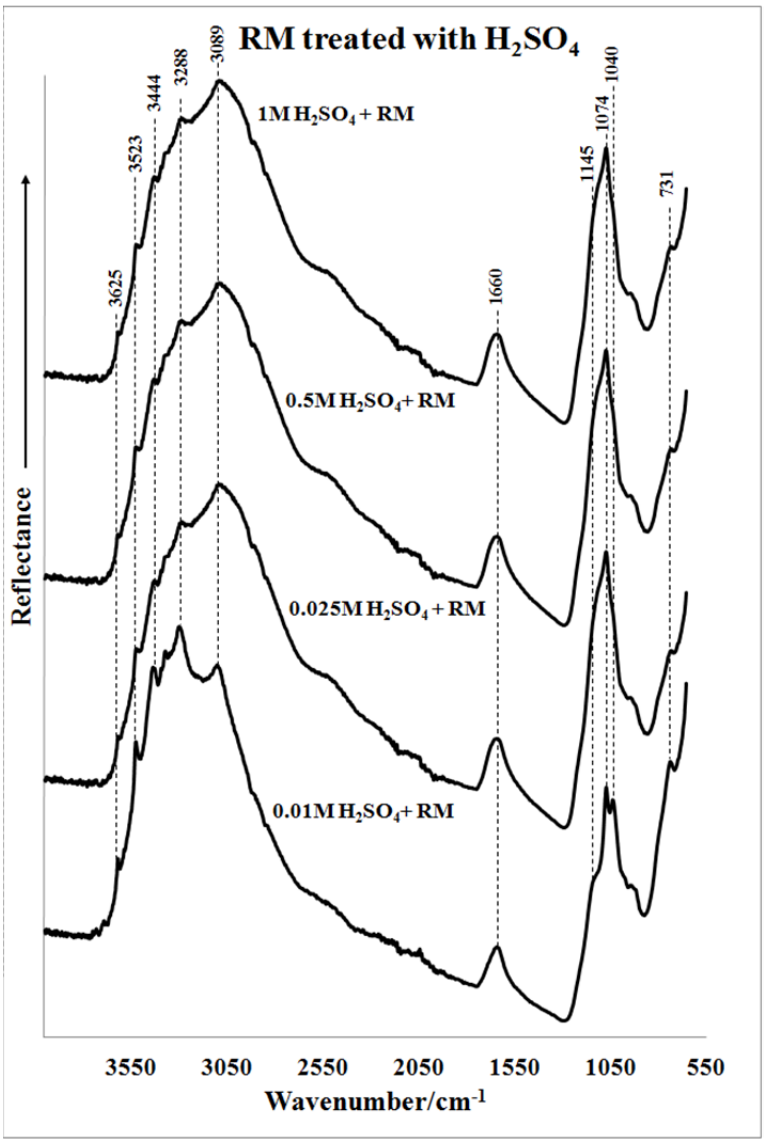

479

480

481

482 **Figure 9**

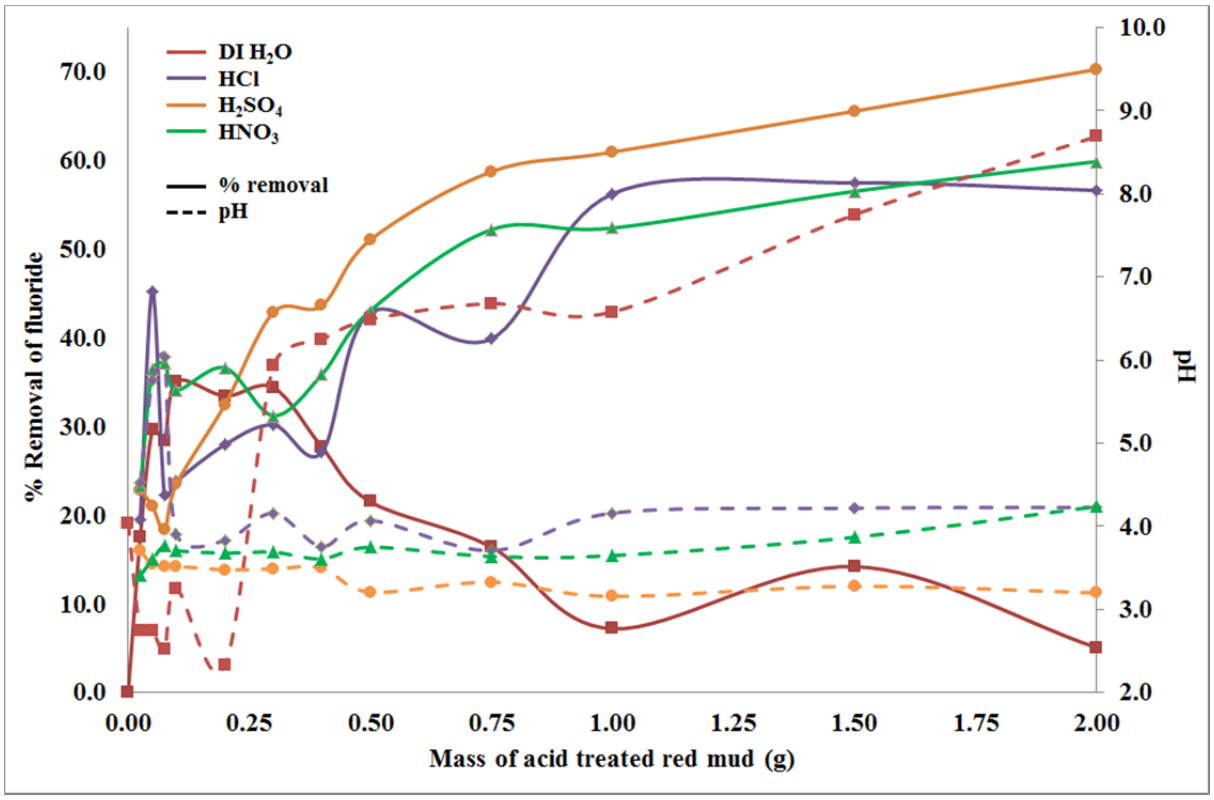

483

484

485 **Figure 10**

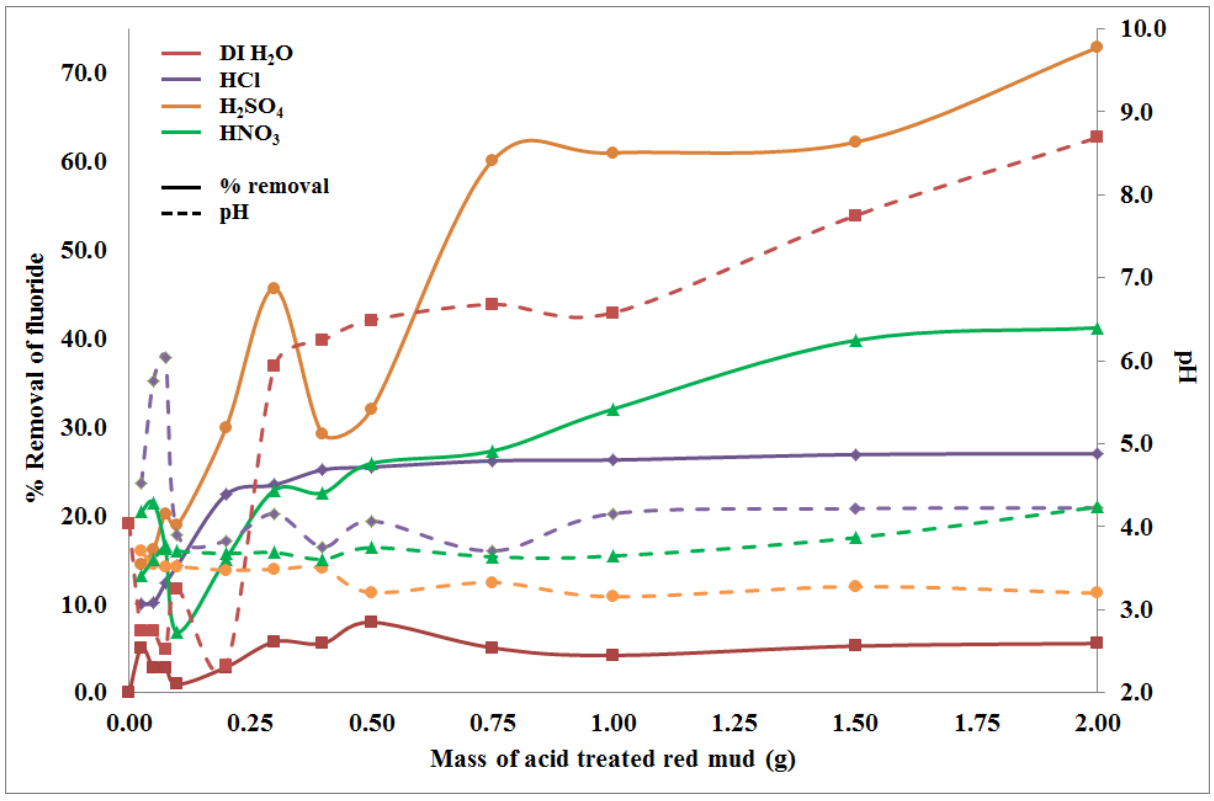

486